LECTURE 9: AEROFOIL THEORY

3.2.1 The Joukowski Transformation

The *Joukowski transformation* is the map

$$z = G(\zeta) = \zeta + \frac{a^2}{\zeta} \tag{3.22}$$

from the complex ζ-plane to the z-plane, where a is a real parameter, which may be taken positive without loss of generality. The mapping $\zeta \mapsto G(\zeta)$ is conformal except at $\zeta = 0$ (where it has a pole) and at the points $\zeta = \pm a$ where $\mathrm{d}G/\mathrm{d}\zeta = 0$.

We can understand the general behaviour of the Joukowski transformation by considering its effect on the circle $|\zeta| = r$ in the ζ-plane. We can parametrise this circle by writing $\zeta = r\mathrm{e}^{\mathrm{i}\theta}$, so that (3.22) becomes

$$z = r\mathrm{e}^{\mathrm{i}\theta} + \frac{a^2}{r}\mathrm{e}^{-\mathrm{i}\theta} = \left(r + \frac{a^2}{r}\right)\cos\theta + \mathrm{i}\left(r - \frac{a^2}{r}\right)\sin\theta. \tag{3.23}$$

Provided $r > a$, this describes an *ellipse* in the z-plane, with principle radii $r + a^2/r$ and $r - a^2/r$. In the limiting case $r \to a$, the ellipse degenerates to a line segment along the real z-axis, namely

$$S = \{z : \operatorname{Im} z = 0, -2a \leqslant \operatorname{Re} z \leqslant 2a\}. \tag{3.24}$$

As r varies between a and ∞, these ellipses sweep out the entire complex z-plane, as shown in Figure 3.8. Hence the exterior of the circle $|\zeta| = a$ in the ζ-plane is mapped by the Joukowski transformation to the exterior of the line segment S.

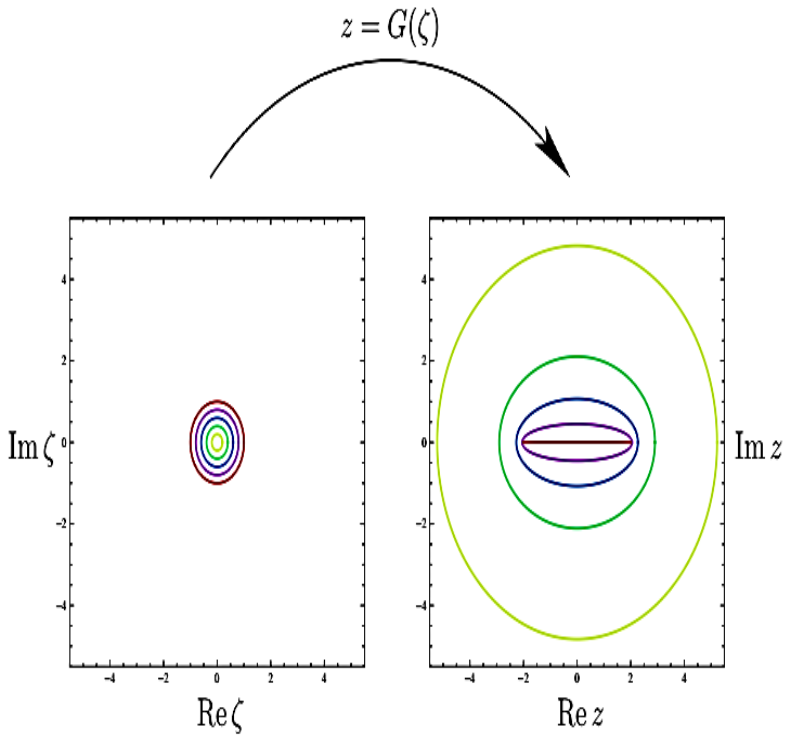

Figure 3.9: The images of circles $|\zeta| = r$ with $r \leqslant a$ under the Joukowski transformation $z = G(\zeta)$ given by (3.22). (Here $a = 1$.)

On the other hand, if $r < a$, (3.23) still parametrises an ellipse in the z-plane, now with principal radii $r + a^2/r$ and $a^2/r - r$ and now described in the clockwise rather than anticlockwise sense. As r varies between 0 and a, these ellipses again fill the entire complex z-plane, as shown in Figure 3.9, so the *interior* of the circle $|\zeta| = a$ also gets mapped to the exterior of the line segment S.

We can invert the Joukowski transformation (3.22) to obtain ζ as a function of z, namely

$$\zeta = \frac{1}{2}\left(z \pm \sqrt{z^2 - 4a^2}\right). \tag{3.25}$$

The square root term in (3.25) may be defined as

$$\sqrt{z^2 - 4a^2} = \sqrt{r_1 r_2}\, \mathrm{e}^{\mathrm{i}(\theta_1+\theta_2)/2}, \tag{3.26}$$

where

$$r_1 = |z - 2a|, \qquad r_2 = |z + 2a|, \qquad \theta_1 = \arg(z - 2a), \qquad \theta_2 = \arg(z + 2a) \tag{3.27}$$

are all shown schematically in Figure 3.10. The ranges for the angles are taken to be $-\pi < \theta_1, \theta_2 \leqslant \pi$, so the multifunction (3.26) is discontinuous across a branch cut along the line segment S on the real-z-axis.

By taking the $+$ or the $-$ in (3.25), we obtain two possible inverses for the mapping $\zeta \mapsto G(\zeta)$, namely

$$\zeta = g_+(z) = \frac{1}{2}\left(z + \sqrt{z^2 - 4a^2}\right), \qquad \zeta = g_-(z) = \frac{1}{2}\left(z - \sqrt{z^2 - 4a^2}\right), \tag{3.28}$$

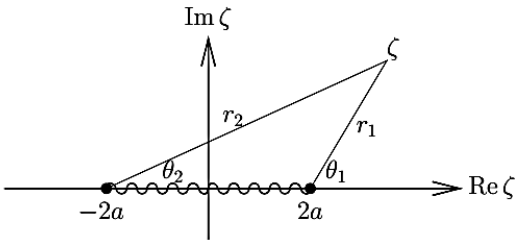

Figure 3.10: The lengths r_1, r_2 and angles θ_1, θ_2 used in the definition (3.26) of $\sqrt{z^2 - 4a^2}$.

both of which are conformal everywhere except on the line segment S. The function $g_+(z)$ maps the exterior of S to the exterior of the circle $|\zeta| = a$, while $g_-(z)$ maps the exterior of S to the interior of the circle $|\zeta| = a$, as indicated in Figure 3.11.

In Figure 3.12, we show the images in the z-plane of various circles in the ζ-plane. The first is the circle $|\zeta| = a$. This passes through the branch points $\zeta = \pm a$ (marked as red dots) where the Joukowski transformation is not conformal, and is mapped to the line segment S, as shown in diagram (i). The second circle, shown in diagram (ii), has a radius larger than a, and its image is thus an ellipse in the z-plane, as explained above. More interesting possibilities occur if we also shift the centre of the circle, as well as its radius. In diagram (iii), we illustrate the application of the Joukowski transformation to a circle whose centre has been slightly offset in the horizontal direction. We have chosen the radius such that the circle passes through one branch point $\zeta = a$, and this causes in a cusp at the corresponding point in the image. Finally, in diagram (iv) we show the result of shifting the circle both horizontally and vertically, while again choosing the radius so that it passes through $\zeta = a$. The resulting image has now lost both left-right and up-down symmetry, and still has a cusp at one end.

The shapes shown in the z-plane in diagrams (iii) and (iv) are examples of so-called *Joukowski aerofoils*. Shapes very similar to these are typically used as the cross-sections of aerofoils and other lifting bodies. They share the key features of a smooth *leading edge* and a sharp *trailing edge*.

The Joukowski transformation can be used to compute the complex potential for flow past any of the shapes shown in Figure 3.12. In this course, we will restrict our attention to case (i), which corresponds to a flat horizontal plate in the z-plane. The other cases are very similar in principle, but involve a few more tedious algebraic complications.

3.2.2 Uniform flow past a flat plate

Suppose fluid flows uniformly at speed U at angle of attack α past a flat plate of length $4a$ occupying the line segment $[-2a, 2a]$ along the real-z-axis. We can use the inverse Joukowski transformation $\zeta = g_+(z)$ to map the fluid onto the exterior of the circle $|\zeta| = a$, as shown schematically in Figure 3.13. The Circle Theorem allows us to calculate the complex potential in the ζ-plane, and the Joukowski transformation

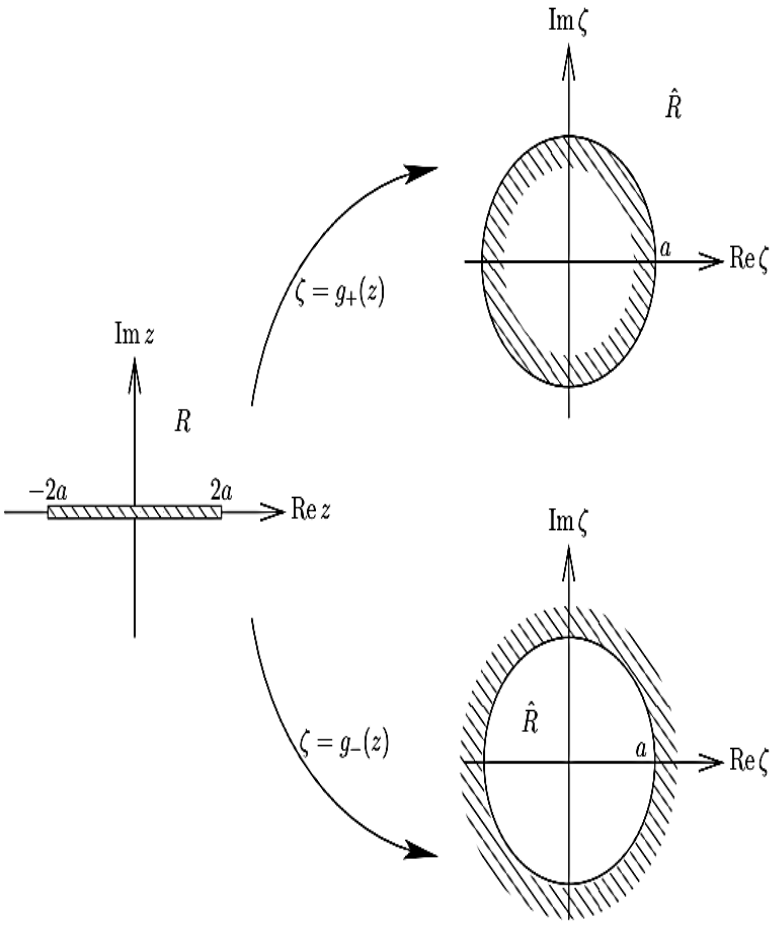

Figure 3.11: Schematic showing the exterior of the line segment $[-2a, 2a]$ along the real-z-axis being transformed by the conformal mappings $\zeta = g_+(z)$ and $\zeta = g_-(z)$ to the outside and inside respectively of the circle $|\zeta| = a$.

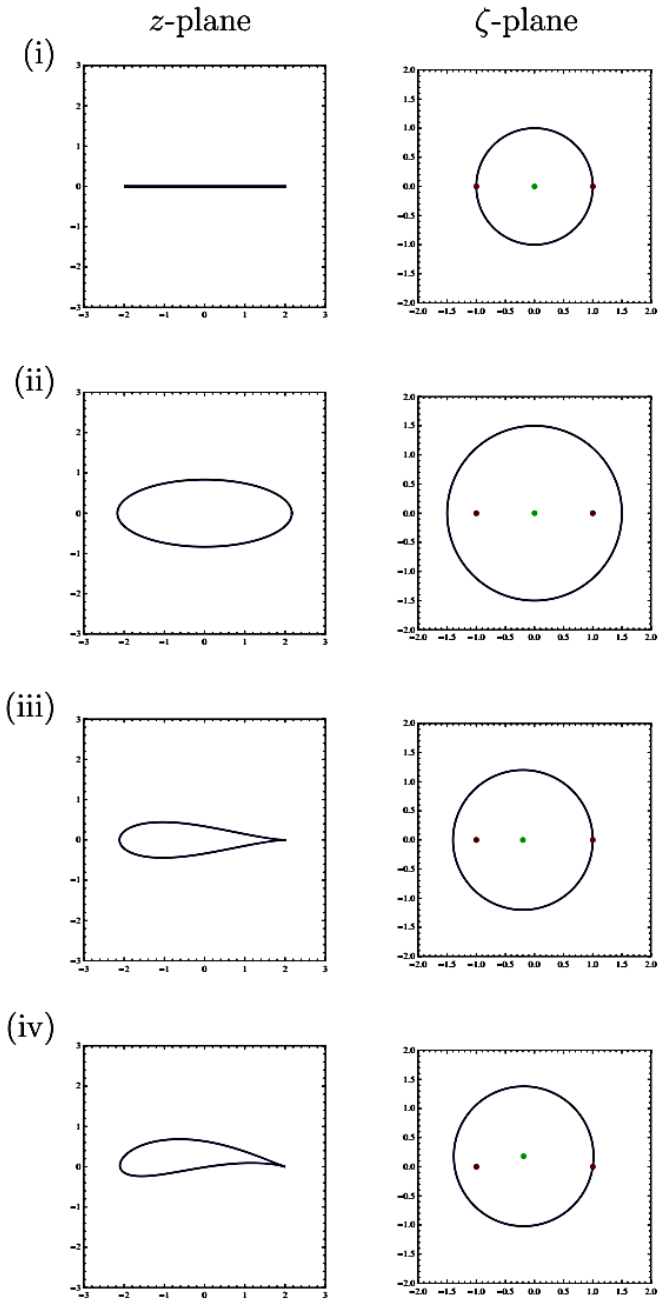

Figure 3.12: The images in the z-plane of four different circles in the ζ-plane under the Joukowski transformation. The centre of each circle is marked with a green dot. The red dots mark the points $\zeta = \pm a$ where the transformation is not conformal. (Here $a = 1$.)

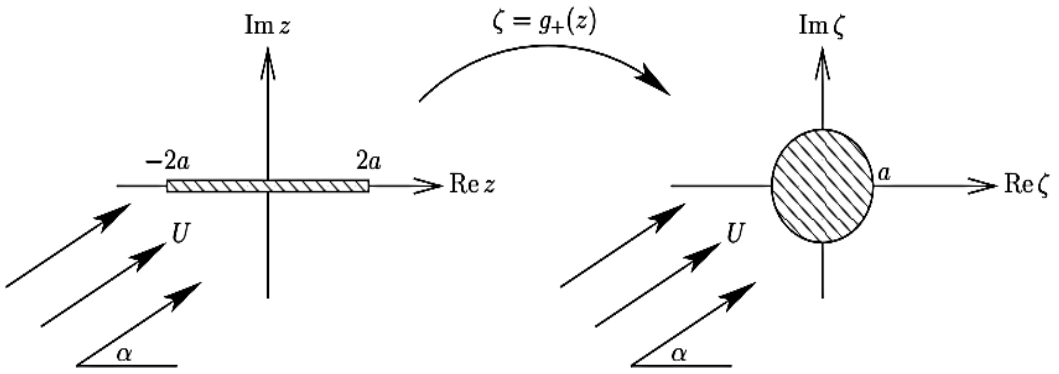

Figure 3.13: Schematic showing uniform flow past a flat plate in the z-plane being transformed to uniform flow past a circle in the ζ-plane by the conformal mapping $\zeta = g_+(z)$.

recovers the corresponding potential in the original z-plane.

Far from the plate, we require the flow to approach a uniform stream, and hence the complex potential should have the far-field behaviour

$$w(z) \sim Uze^{-i\alpha} \quad \text{as } z \to \infty. \tag{3.29}$$

We note from (3.22) and (3.25) that $\zeta \sim z$ as $z \to \infty$, and we therefore impose the corresponding behaviour

$$W(\zeta) \sim U\zeta e^{-i\alpha} \quad \text{as } \zeta \to \infty \tag{3.30}$$

on the complex potential in the ζ-plane.

Now the Circle Theorem, with background potential $f(\zeta) = U\zeta e^{-i\alpha}$, gives us the full complex potential in the ζ-plane, namely

$$W(\zeta) = U\zeta e^{-i\alpha} + \frac{Ua^2 e^{i\alpha}}{\zeta}. \tag{3.31}$$

The complex potential in the z-plane is given implicitly by (3.31) and the Joukowski mapping (3.22), and elimination of ζ leads to

$$\begin{aligned} w(z) &= \frac{Ue^{-i\alpha}}{2}\left(z + \sqrt{z^2 - 4a^2}\right) + \frac{Ue^{i\alpha}}{2}\left(z - \sqrt{z^2 - 4a^2}\right) \\ &= Uz\cos\alpha - iU\sqrt{z^2 - 4a^2}\,\sin\alpha. \end{aligned} \tag{3.32}$$

The velocity components are given by

$$u - iv = \frac{dw}{dz} = U\cos\alpha - \frac{iUz\sin\alpha}{\sqrt{z^2 - 4a^2}}. \tag{3.33}$$

The streamlines for the resulting flow are shown in Figure 3.14. We see that the flow is symmetric and the velocity is zero at two stagnation points $z = \pm 2a\cos\alpha$ on the plate.

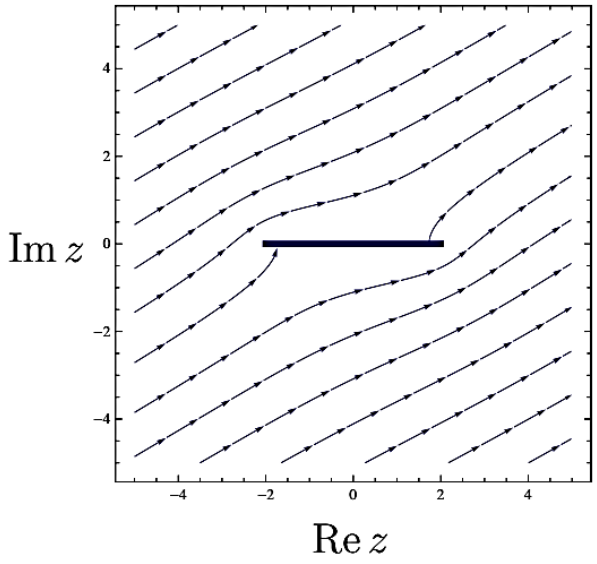

Figure 3.14: The streamlines for uniform flow with angle of attack α past a flat plate of length $4a$. (Here $\alpha = \pi/6$ and $a = 1$.)

We can incorporate a circulation Γ by inserting a vortex at the centre of the circle in the ζ-plane as usual, resulting in

$$W(\zeta) = U\zeta \mathrm{e}^{-\mathrm{i}\alpha} + \frac{Ua^2\mathrm{e}^{\mathrm{i}\alpha}}{\zeta} - \frac{\mathrm{i}\Gamma}{2\pi}\log\zeta. \tag{3.34}$$

Again we can eliminate ζ to obtain the complex potential $w(z)$ in the z-plane, although in practice this may not be worthwhile. We can instead calculate the velocity components by using the chain rule:

$$\begin{aligned} u - \mathrm{i}v = \frac{\mathrm{d}w}{\mathrm{d}z} &= \frac{\mathrm{d}W}{\mathrm{d}\zeta} \Big/ \frac{\mathrm{d}z}{\mathrm{d}\zeta} \\ &= \frac{U\mathrm{e}^{-\mathrm{i}\alpha} - \dfrac{Ua^2\mathrm{e}^{\mathrm{i}\alpha}}{\zeta^2} - \dfrac{\mathrm{i}\Gamma}{2\pi\zeta}}{1 - \dfrac{a^2}{\zeta^2}} \\ &= \frac{U\mathrm{e}^{-\mathrm{i}\alpha}\zeta^2 - \mathrm{i}(\Gamma/2\pi)\zeta - Ua^2\mathrm{e}^{\mathrm{i}\alpha}}{\zeta^2 - a^2}. \end{aligned} \tag{3.35}$$

Now the stagnation points in the ζ-plane are given by

$$\frac{\zeta}{a} = \mathrm{e}^{\mathrm{i}\alpha}\left(\mathrm{i}\gamma \pm \sqrt{1-\gamma^2}\right), \tag{3.36}$$

where we recall the shorthand $\gamma = \Gamma/4\pi Ua$. Provided $\gamma \in (-1,1)$, there are two stagnation points, both lying on the circle $|\zeta| = a$. We use the Joukowski transformation (3.22) to map these back to two stagnation points on the plate in the z-plane given by

$$z = 2a\left(-\gamma \sin\alpha \pm \sqrt{1-\gamma^2}\cos\alpha\right). \tag{3.37}$$

We see that these revert to their zero-circulation positions $z = \pm 2a\cos\alpha$ when $\gamma = 0$.

Alternatively, we can eliminate ζ to write the complex potential in the z-plane as

$$Uz\cos\alpha - \mathrm{i}U\sqrt{z^2-4a^2}\sin\alpha - \frac{\mathrm{i}\Gamma}{2\pi}\log\left(\frac{z+\sqrt{z^2-4a^2}}{2}\right). \tag{3.38}$$

Now differentiation with respect to z and simplification leads to

$$u - \mathrm{i}v = \frac{\mathrm{d}w}{\mathrm{d}z} = U\cos\alpha - \frac{\mathrm{i}}{\sqrt{z^2-4a^2}}\left(\frac{\Gamma}{2\pi} + Uz\sin\alpha\right). \tag{3.39}$$

3.2.3 The Kutta condition

We can see from equation (3.39) that the velocity is in general unbounded at the two edges of the plate $z = \pm 2a$. In practice, viscous effects will come into play in a neighbourhood of the edges of the plate to ensure that the velocity remains finite. With these effects included, it turns out to be impossible for the fluid to bend around the trailing edge of the plate, as indicated by Figure 3.14. Instead it must separate smoothly as shown in Figure 3.15, and this selects a particular value of the circulation Γ. The *Kutta condition* states that the circulation must be chosen such that *the velocity at the trailing edge is finite.*

Returning to equation (3.39), we see that the velocity at the trailing edge can be finite only if the final bracketed term tends to zero as $z \to 2a$, and this implies that the circulation must be given by

$$\Gamma = -4\pi Ua\sin\alpha. \tag{3.40}$$

Having made this choice, we can then evaluate the velocity at the trailing edge from (3.39), for example by using l'Hôpital's rule:

$$u - \mathrm{i}v\big|_{z=2a} = \left.\frac{\mathrm{d}w}{\mathrm{d}z}\right|_{z=2a} = U\cos\alpha. \tag{3.41}$$

Hence we see that the fluid velocity is tangent to the plate at the trailing edge, as shown in Figure 3.15.

Of course, the velocity is still unbounded at the *leading* edge of the plate $z = -2a$. This is a problem with flow past a flat plate, and partly explains why flat plates do not make particularly good aerofoils. More realistic aerofoil shapes have a smooth leading edge and a sharp trailing edge, like those shown in Figure 3.12(iii) and (iv). For such shapes, the Kutta condition gives rise to a velocity field that is bounded everywhere.

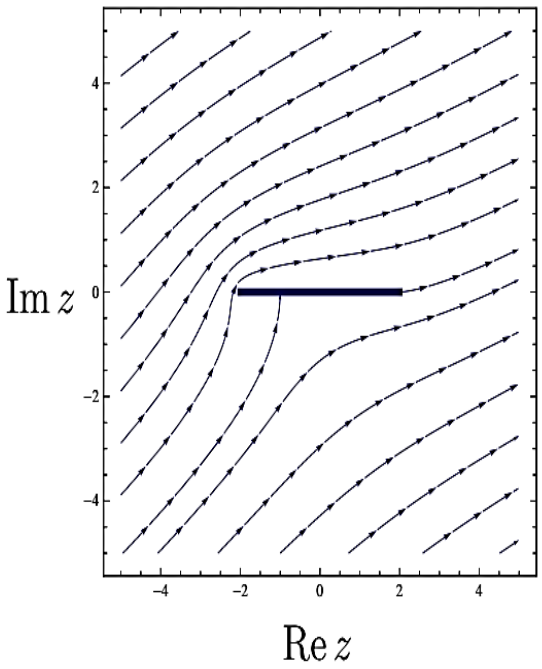

Figure 3.15: The streamlines for uniform flow with angle of attack α past a flat plate of length $4a$, with circulation given by (3.40) to satisfy the Kutta condition. (Here $\alpha = \pi/6$ and $a = 1$.)

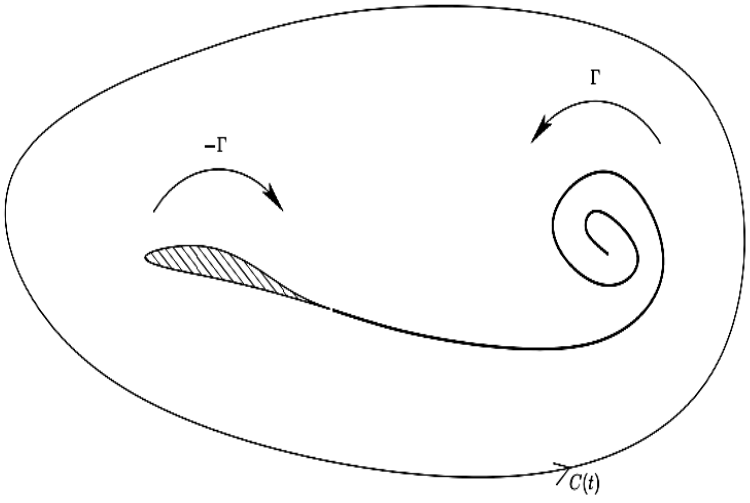

Figure 3.16: Schematic of a trailing vortex behind an aerofoil. The material curve $C(t)$ encloses both the vortex and the aerofoil.

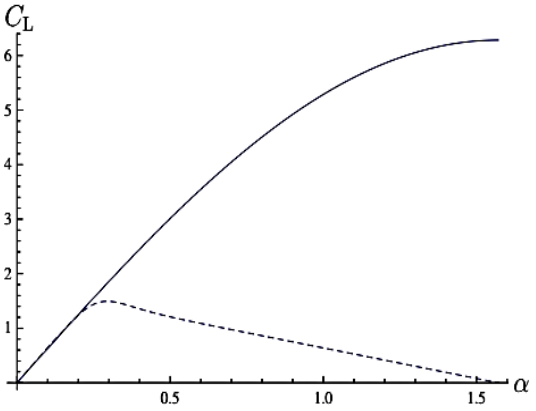

Figure 3.17: Lift coefficient C_L for a flat plate versus angle of attack α. The solid curve shows the theoretical prediction $C_L = 2\pi \sin\alpha$ implied by (3.42); the dashed curve shows schematically typical experimental results.

We recall from Kelvin's Circulation Theorem that the circulation around a closed material curve $C(t)$ is constant in time. This raises the question: how did the circulation (3.40) around the plate arise in the first place? The answer is that, as an aerofoil accelerates from rest, the Kutta condition forces it to shed a *starting vortex*, as shown schematically in Figure 3.16.[2] By applying Kelvin's Theorem to a large contour $C(t)$ that encloses both the aerofoil and the starting vortex, we deduce that there must be a circulation around the aerofoil equal and opposite to that around the starting vortex.

Once we have used the Kutta condition to determine the circulation around an aerofoil, we can apply the Kutta–Joukowski Lift Theorem to calculate the lift and drag forces, namely $L = -\rho U\Gamma$, $D = 0$. For a flat plate, the circulation is given by equation (3.40), and the resulting lift force is therefore given by

$$L = 4\pi\rho U^2 a \sin\alpha. \tag{3.42}$$

Wind-tunnel experiments show that this formula works very well provided the angle of attack α is smaller than about $\pi/12$. If α is increased any further, the lift rapidly decreases to virtually zero, and the aerofoil *stalls*. This is caused by the formation of a turbulent wake downstream of the aerofoil.

We illustrate this behaviour in Figure 3.17. The lift on the plate is measured by the dimensionless *lift coefficient*

$$C_L = \frac{L}{2\rho U^2 a}, \tag{3.43}$$

where equation (3.42) implies that $C_L = 2\pi \sin\alpha$. As shown by the solid curve in Figure 3.17, the theoretically predicted lift increases with the angle of attack, attaining its maximum value as $\alpha \to \pi/2$. However, it is intuitively clear that the lift should be zero when the plate is aligned transverse to the flow. Typical experimental results are shown schematically by the dashed curve.

[2]These vortices dictate the time delay between aeroplanes taking off from a busy airport.